

Effect of Zn Concentration on the Microstructure and Mechanical Properties of Al-Mg-Si-Zn Alloys Processed by Gravity Die Casting



LONGFEI LI, SHOUXUN JI, QIANG ZHU, YUN WANG, XIXI DONG,
WENCHAO YANG, STEPHEN MIDSON, and YONGLIN KANG

The microstructure and mechanical properties of Al-8.1Mg-2.6Si-(0.08 to 4.62)Zn alloys (in wt pct) have been investigated by the permanent mold casting process. X-ray diffraction analysis shows that the τ -Mg₃₂(Al, Zn)₄₉ phase forms when the Zn content is 1.01 wt pct. With higher Zn contents of 2.37 and 3.59 wt pct, the η -MgZn₂ and τ -Mg₃₂(Al, Zn)₄₉ phases precipitate in the microstructure, and the η -MgZn₂ phase forms when the Zn content is 4.62 wt pct. Metallurgical analysis shows that the η -MgZn₂ and τ -Mg₃₂(Al, Zn)₄₉ phases strengthen the Al-8.1Mg-2.6Si-(0.08 to 4.62)Zn alloys. After solutionizing at 510 °C for 180 minutes and aging at 180 °C for 90 minutes, the η' -MgZn₂ phase precipitates in the α -Al matrix, which significantly enhances the mechanical properties. Addition of 3.59 wt pct Zn to the Al-8.1Mg-2.6Si alloy with heat treatment increases the yield strength from 96 to 280 MPa, increases the ultimate tensile strength from 267 to 310 MPa, and decreases the elongation from 9.97 to 1.74 pct.

<https://doi.org/10.1007/s11661-018-4684-2>
© The Author(s) 2018

I. INTRODUCTION

ALUMINUM alloys are widely used to produce castings with complex external geometries and internal cavities,^[1,2] and they have the advantages of low density and good mechanical properties. This is attractive for transport because lightweight structures are beneficial for reduction of CO₂ emissions.^[3,4] Currently, Al-Si-Mg (Cu) alloys are the main materials used to produce casting components with good mechanical properties by either gravity die casting or low-pressure die casting.^[5,6] Several strengthening phases have been reported for

Al-Si-Mg (Cu) alloys. Ouellet and Samuel^[7] found that the Al-Si-Cu alloy (319 type) is strengthened by θ' and β' precipitates formed after heat treatment. Wiengmoon *et al.*^[8] found that the θ'' and θ' -Al₃Cu phases are responsible for the precipitate hardening of 319 alloys. However, Jahn *et al.*^[9] found that the quaternary Q' (containing Al, Mg, Si, and Cu) and S' (containing Al, Mg, and Cu) phases are the key precipitates in the cast 319 alloys. Hwang *et al.*^[10] identified θ and Q precipitates in the 319-type Al-Si-Cu alloy. Mishra *et al.*^[11] found that the ternary S' (Al₂CuMg type) phase strengthens 339-type aluminum castings.

On the other hand, Al-Zn-Mg alloys are used to manufacture high-strength components. Owing to fine-scale precipitation of metastable Zn- and Mg-rich phases, the strength of Al-Zn-Mg-Cu alloys can reach a level of 650 MPa for the yield strength and 700 MPa for the UTS after aging at 120 °C for 24 hours.^[12] Yang *et al.*^[13] investigated an Al-Zn-Mg alloy with a Mg-to-Zn atomic ratio of 0.34 to improve the strength through formation of the coherent polyhedral τ -phase [(Al, Zn)₄₉Mg₃₂]. Li *et al.*^[14] investigated solution treatment of the microalloyed Al-Zn-Mg alloy system with Sc and Zr and found that both η' -MgZn₂ precipitates and fine Al₃(Sc, Zr) particles are homogeneously distributed throughout the α -Al grains under heat-treatment conditions. This alloy has a yield strength of 560 MPa, an UTS of 580 MPa, and an elongation of 10 pct. Shin *et al.*^[15] studied Al-Zn-Mg alloys with high

LONGFEI LI is with the Brunel Centre for Advanced Solidification Technology (BCAST), Institute of Materials and Manufacturing, Brunel University London, Uxbridge, Middlesex UB8 3PH and with the General Research Institute for Nonferrous Metals, Beijing 100088, China and also with the University of Science and Technology Beijing, Beijing 100083, China. SHOUXUN JI, YUN WANG, and XIXI DONG are with the Brunel Centre for Advanced Solidification Technology (BCAST), Institute of Materials and Manufacturing. Contact email: shouxun.ji@brunel.ac.uk QIANG ZHU is with the Southern University of Science and Technology, Shenzhen 518055, China. Contact e-mail: zhuq@sustc.edu.cn WENCHAO YANG is with the State Key Laboratory of Solidification Processing, Northwestern Polytechnical University, Xi'an 710072, China. STEPHAN MIDSON is with the General Research Institute for Nonferrous Metals and also with the Colorado School of Mines, Golden, CO 80401. YONGLIN KANG is with the University of Science and Technology Beijing.

Manuscript submitted November 28, 2017.

Article published online June 8, 2018

Zn contents and found that the UTS can reach higher than 470 MPa for die castings. They attributed the high strength to the very fine lamellar structure of Zn-rich phases within the α -Al matrix.

In general, Al-Si-Mg (Cu) alloys have better castability than Al-Zn-Mg (Cu) alloys. Ji *et al.*^[16,17] developed a high-strength Al-Mg₂Si-Mg-Zn alloy for high-pressure die casting. Solution and aging treatment for a short time resulted in a significant improvement in the mechanical properties,^[18] and the alloy has been used for shaped components in aerospace manufacturing.^[19] Similarly, Yan *et al.*^[20] found that the mechanical properties of Al-Mg-Si-Cu alloys are enhanced by Zn addition, yielding an alloy with a yield strength of 270 MPa, an UTS of 335 MPa, and an elongation of 26.5 pct. Ding *et al.*^[21] also found that the addition of 3.0 wt pct Zn can significantly enhance age hardening of Al-Mg-Si alloys. Therefore, it is worthwhile investigating the effect of Zn addition to Al-Mg-Si alloys processed by gravity die casting, the improvement in the properties, and the strengthening mechanism.

In this study, the effect of Zn concentration on the microstructure and mechanical properties of Al-8.1 wt pct Mg-2.6 wt pct Si-(0.08 to 4.62) wt pct Zn alloys processed by gravity die casting was investigated under both the as-cast and heat-treated conditions. Phase formation, the microstructural characteristics, and the correlation between the microstructure and the mechanical properties of the alloys were characterized for different Zn concentrations.

II. EXPERIMENTAL

Al-8.1 wt pct Mg-2.6 wt pct Si (hereafter denoted Al-Mg-Si) alloys with different levels of Zn addition (hereafter denoted Al-Mg-Si-Zn) were prepared from pure Al, Mg, Zn, and Al-50 wt pct Si master alloys. Each element was loaded into a clay-graphite crucible (capacity of 30 kg) at a calculated ratio considering the additional contents of burning loss. During melting in an electric resistance furnace, the temperature of the melt was controlled at 730 ± 5 °C. Pure Al and Al-50 wt pct Si were melted before adding pure Mg and Zn ingots. Beryllium (20 ppm) was added to the melt to reduce oxidization of Mg. When the melt was homogenized to 730 ± 5 °C, a rotary degassing unit was used to inject pure Ar into the melt for 3 minutes, and the melt was held in the furnace for 30 minutes to

provide time for the floating dross and impurities to reach the melt surface. Samples for composition testing were obtained by pouring the melt into a mushroom-like mold. The compositions of the alloys were measured by an optical mass spectroscope (OMS), in which five sparks were tested to obtain the average composition of each alloy. The compositions of the alloys are given in Table I.

After analyzing the compositions with the OMS, the melts were cooled to 710 °C and poured into a gravity mold. Before pouring, the surfaces of the molds were coated with boron nitride and preheated to 350 °C. Figure 1 shows a photograph of a complete casting, along with the dimensions of the tensile test samples. At least five castings were made for each alloy for microstructural characterization and tensile property testing.

During solution treatment at 510 °C, the temperature of the furnace was recorded by a thermocouple with ± 1 °C accuracy. Different holding times (0 to 420 minutes) were evaluated. After solution treatment, the tensile test samples were immediately water quenched and then subjected to aging at 180 °C for 90 minutes.

The tensile tests were performed with an Instron 5500 Universal Electromechanical Testing System. The cross-head speed used for the tensile tests was 2 mm min^{-1} . At least five samples were tested to determine the mechanical properties.

X-ray diffraction (XRD) was performed with a SmartLab high-resolution X-ray diffractometer using Cu K α radiation. The XRD spectra were analyzed using MDI Jade 6.0 software containing the PDF database. The samples for microstructural examination were obtained from the middle of the tensile test samples. At least ten fields of view for microstructural examination were randomly chosen for metallurgical analysis. The microstructures were characterized by optical microscopy (Zeiss) and scanning electron microscopy (SEM, SUPRA 35VP) with energy dispersive spectroscopy (EDS). The specimens for transmission electron microscopy (TEM) were prepared using slices of the alloys, which were mechanically ground to about 70 μm in thickness followed by ion beam thinning using a Gatan precision ion polishing system at 5.0 kV with an incident angle of 4 deg. TEM was performed using a JEOL-2100 transmission electron microscope equipped with an EDS system operating at an accelerating voltage of 200 kV.

Table I. Compositions of Cast Al-Mg-Si-Zn Alloys with Different Zn Contents (Weight Percent)

Alloys	Mg	Si	Zn	Fe	Be (Ppm)	Others	Al
Al-Mg-Si	8.11	2.61	0.08	0.15	20	< 0.10	bal.
Al-Mg-Si-Zn	8.05	2.65	1.01	0.11	22	< 0.10	bal.
Al-Mg-Si-Zn	8.15	2.68	2.37	0.18	18	< 0.10	bal.
Al-Mg-Si-Zn	8.10	2.62	3.59	0.12	25	< 0.10	bal.
Al-Mg-Si-Zn	8.13	2.66	4.62	0.16	21	< 0.10	bal.

III. RESULTS

A. Effect of Zn on the Al-Mg-Si Alloy in the As-cast Condition

Figure 2 shows the as-cast microstructure of the Al-Mg-Si alloy. Figure 2(a) presents an optical image showing a hypoeutectic microstructure consisting of primary α -Al dendrites, Al-Mg₂Si eutectics, and Fe-rich intermetallic. From metallurgical analysis, the volume fractions of the primary α -Al, Al-Mg₂Si eutectic and Fe-rich intermetallic phases are 55.0, 44.6, and 0.4 pct, respectively. The backscattered SEM image in Figure 2(b) shows that the eutectic Mg₂Si phase has a lamellar morphology. The average spacing of the Al-Mg₂Si eutectic measured by the transversal method

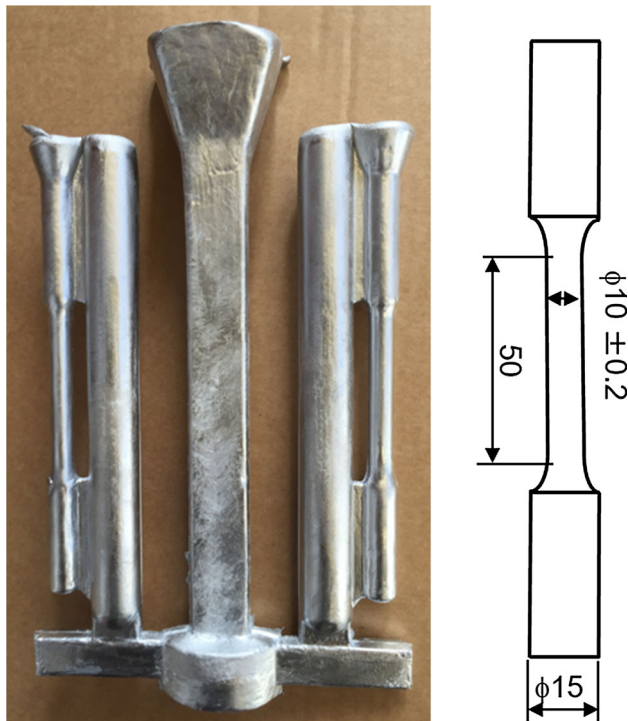


Fig. 1—Permanent mold casting fabricated according to ASTM B-108 and the key dimensions of the tensile test bars.

using Image-Pro Plus 6.0 is $1.76 \pm 0.28 \mu\text{m}$, which is the average distance between the center lines of two adjacent Mg₂Si phases. The Fe-rich intermetallic phase is located at the boundaries of the primary α -Al dendrites and Al-Mg₂Si eutectic and has an irregular shape. SEM/EDS analysis [Figure 3(b)] shows that the Fe-rich intermetallic phase is Al₃Fe, which forms at a relatively low cooling rate,^[22,23] rather than β -AlFeSi, which forms at a relatively high cooling rate.^[24]

Figure 4 shows the as-cast microstructures of Al-Mg-Si-Zn alloys containing different Zn contents. Similar to the microstructure in Figure 2, the alloy with 1.01 wt pct Zn consists of the primary α -Al phase, Al-Mg₂Si eutectic phase, and Fe-rich intermetallic phase [Figure 4(a)]. When the Zn content is increased to 2.37 wt pct, the AlMgZn intermetallic phase is observed at the boundaries of the α -Al grains [marked in Figure 4(b)]. Upon further increasing in the Zn content to 3.59 and 4.62 wt pct, the AlMgZn intermetallic phase becomes coarse with an irregular morphology, as shown in Figures 4(c) and (d). The volume fraction and the average area of the AlMgZn intermetallic phase were measured as a function of the Zn concentration using Image-Pro Plus 6.0, as shown in Figures 5 and 6. The volume fraction of the AlMgZn intermetallic phase initially increases with increasing Zn content but levels off at 3.7 pct. The average area generally increases with the increasing Zn content to $21.80 \mu\text{m}^2$ at 4.62 wt pct Zn.

The compositions of the AlMgZn intermetallic phase in the Al-Mg-Si-Zn alloys with different Zn concentrations are given in Table II. When the Zn contents are 2.37 and 3.59 wt pct, the atomic ratio of Zn/Mg in the AlMgZn intermetallic phase is the same (Zn/Mg = 0.8). However, the ratio increases to 1.1 when the Zn content is 4.62 wt pct. This can be explained by the XRD patterns of the as-cast Al-Mg-Si-Zn alloys (Figure 7). The Mg₃₂(Al, Zn)₄₉ phase is observed with 1.01 wt pct Zn addition. However, both the Mg₃₂(Al, Zn)₄₉ and MgZn₂ phases are present when the Zn contents are 2.37 and 3.59 wt pct, and the MgZn₂ phase is the only intermetallic when the Zn content further increases to 4.62 wt pct. This confirms that the variation in the Zn/Mg atomic ratio is associated with the different intermetallic phases in the alloys.

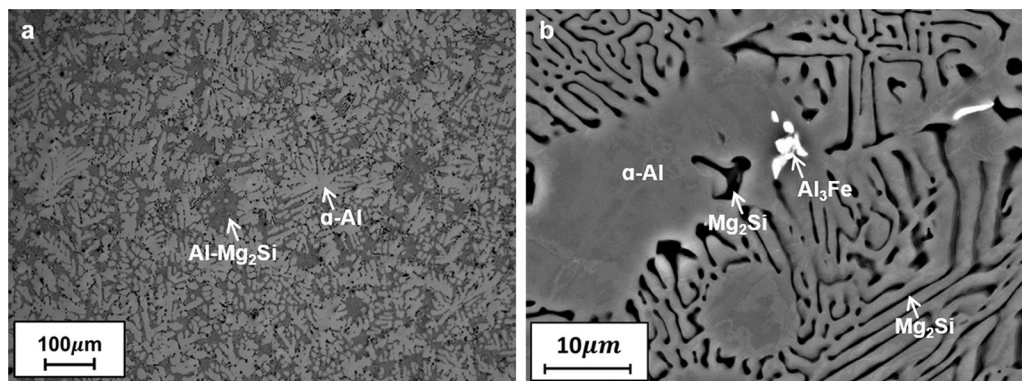


Fig. 2—(a) Optical and (b) backscattered SEM image showing the as-cast microstructure of the Al-Mg-Si alloy.

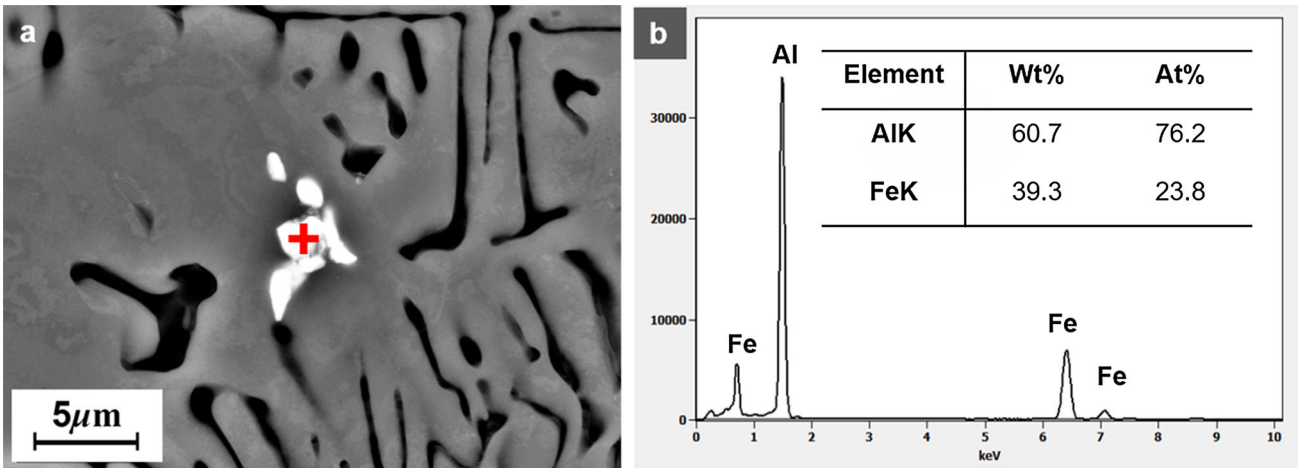


Fig. 3—(a) Backscattered SEM image and (b) the corresponding EDS analysis of the Fe-rich intermetallic phase in the Al-Mg-Si alloy in the as-cast condition.

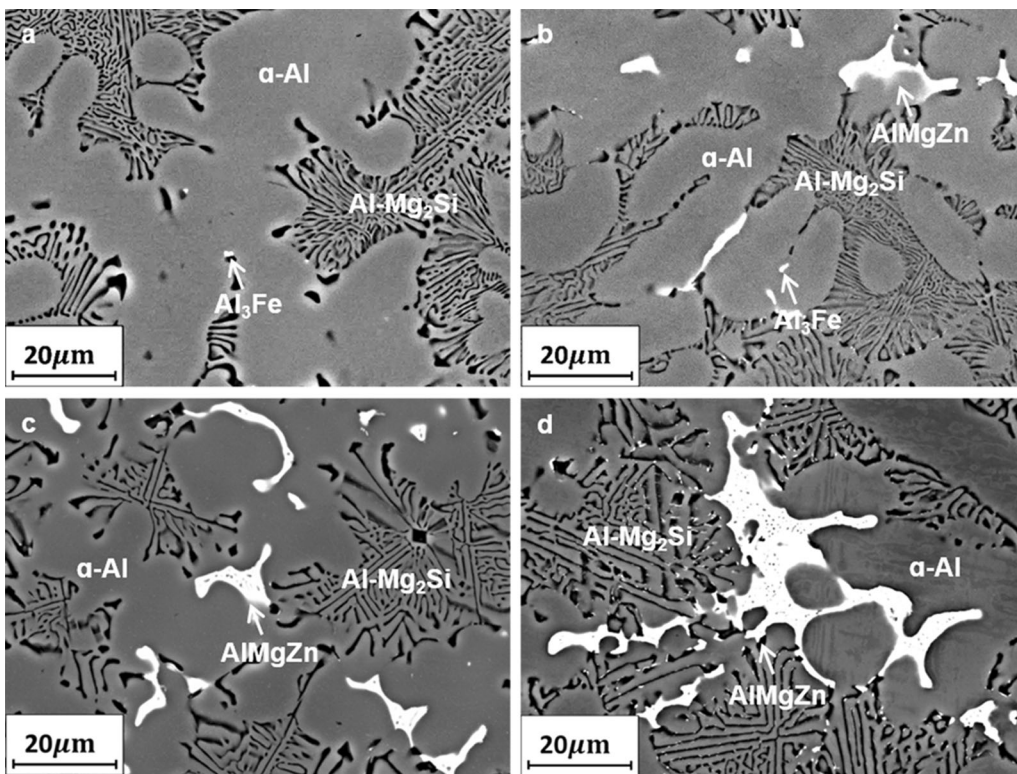


Fig. 4—Backscattered SEM images showing the as-cast microstructures of the Al-Mg-Si-Zn alloys with (a) 1.01, (b) 2.37, (c) 3.59, and (d) 4.62 wt pct Zn.

Figure 8 shows the effect of the Zn content on the tensile properties of the Al-Mg-Si-Zn alloy in the as-cast condition. When the Zn content increases from 1.01 to 4.62 wt pct, the yield strength increases from 108 to 185 MPa and elongation decreases from 2.47 to 1.06 pct, while the UTS is generally constant at about 230 MPa. However, the Al-Mg-Si-Zn alloy with high Zn content (4.62 wt pct) shows severe hot tearing during casting and has low ductility. High hot tearing susceptibility is undesirable in gravity die casting.^[25,26] Therefore, based on the combination of the mechanical

properties and castability, the Al-Mg-Si-Zn alloy with 3.59 wt pct Zn was selected for further heat treatment.

B. Effect of the Zn Content in the Heat-Treated Condition

Figure 9 shows the effect of solution treatment on the microstructure of the Al-Mg-Si-Zn alloy containing 3.59 wt pct Zn. Most of the AlMgZn intermetallic phase dissolves in the primary α -Al phase after soaking at 510 °C for 10 minutes [Figure 9(b)]. The AlMgZn

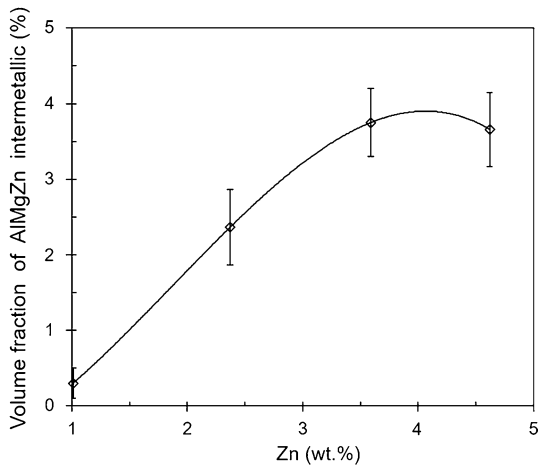


Fig. 5—Effect of the Zn content on the volume fraction of the AlMgZn intermetallic in the Al-Mg-Si-Zn alloy.

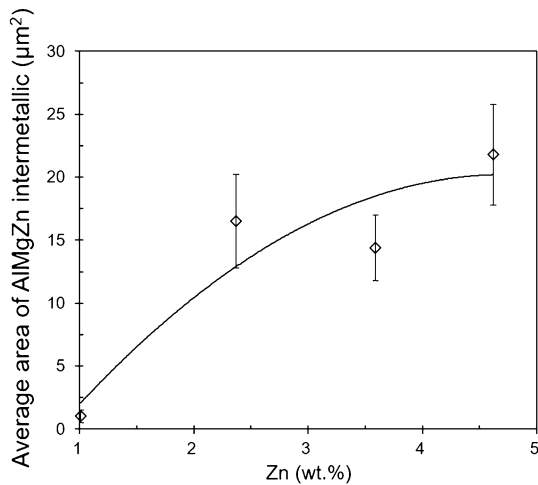


Fig. 6—Effect of the Zn content on the average area of the AlMgZn intermetallic in the Al-Mg-Si-Zn alloy.

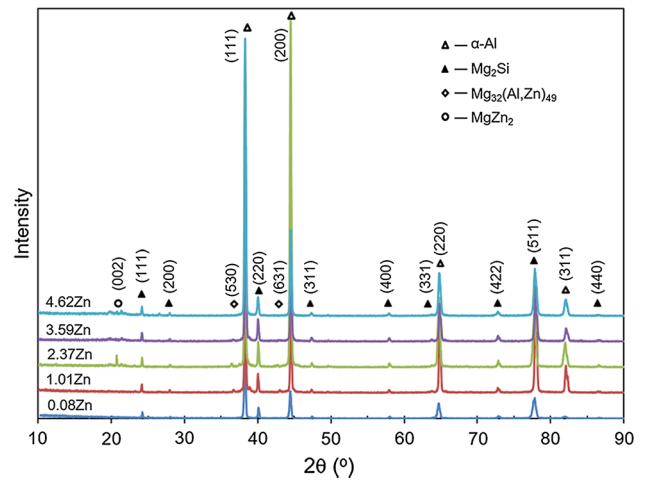


Fig. 7—XRD patterns of the Al-Mg-Si-Zn alloys in the as-cast condition.

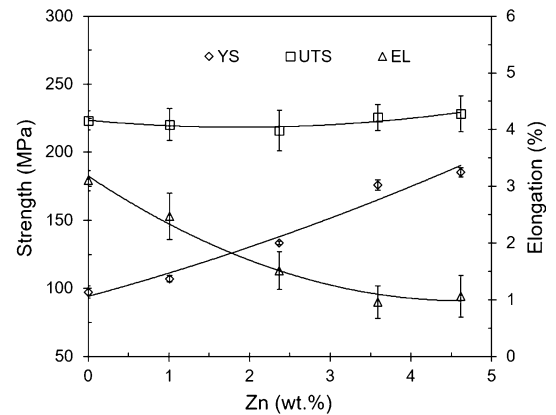


Fig. 8—Effect of the Zn content on the tensile properties of the Al-Mg-Si-Zn alloy in the as-cast condition (YS = yield strength, UTS = ultimate tensile strength, EL = elongation).

Table II. SEM/EDS Quantitative Analysis of the AlMgZn Intermetallic Phase in Al-Mg-Si-Zn Alloys with Different Zn Contents

Zn (Wt Pct)	Morphology	Compounds	Mg (At. Pct)	Zn (At. Pct)	Al (At. Pct)
2.37	irregular	Al _{4.8} MgZn _{0.8}	15.2	12.2	72.6
3.59	irregular	Al _{4.8} MgZn _{0.8}	15.5	12.2	72.3
4.62	irregular	Al _{7.6} MgZn _{1.1}	10.3	11.3	78.4

intermetallic phase completely dissolves with longer solution-treatment time [Figure 9(c)]. This is supported by the XRD pattern shown in Figure 10, in which the peaks for Mg₃₂(Al, Zn)₄₉ and MgZn₂ disappear after soaking at 510 °C for 10 minutes.

The morphology of the Mg₂Si phase changes after solution treatment, but significant spheroidization of the Mg₂Si phase does not occur when the soaking time is less than 60 minutes. After soaking at 510 °C for 180 minutes, the Mg₂Si phase completely spheroidizes. Furthermore, solution treatment does not cause any obvious changes in the irregular morphology of the

Al₃Fe intermetallic phase (identified in Figure 9) or the shape of the primary α-Al phase. To confirm the above observation, the Mg₂Si- and Fe-rich intermetallic phases after soaking at 510 °C for 180 minutes were further investigated by TEM, and the results are shown in Figure 11. From the TEM images, the Al₃Fe intermetallic phase exhibits a long-plate morphology with sharp corners. However, the Mg₂Si phase has an oval morphology, which is significantly different from its morphology in the as-cast condition. Therefore, solution treatment results in dissolution of the AlMgZn intermetallic phase and spheroidization of the Mg₂Si phase.

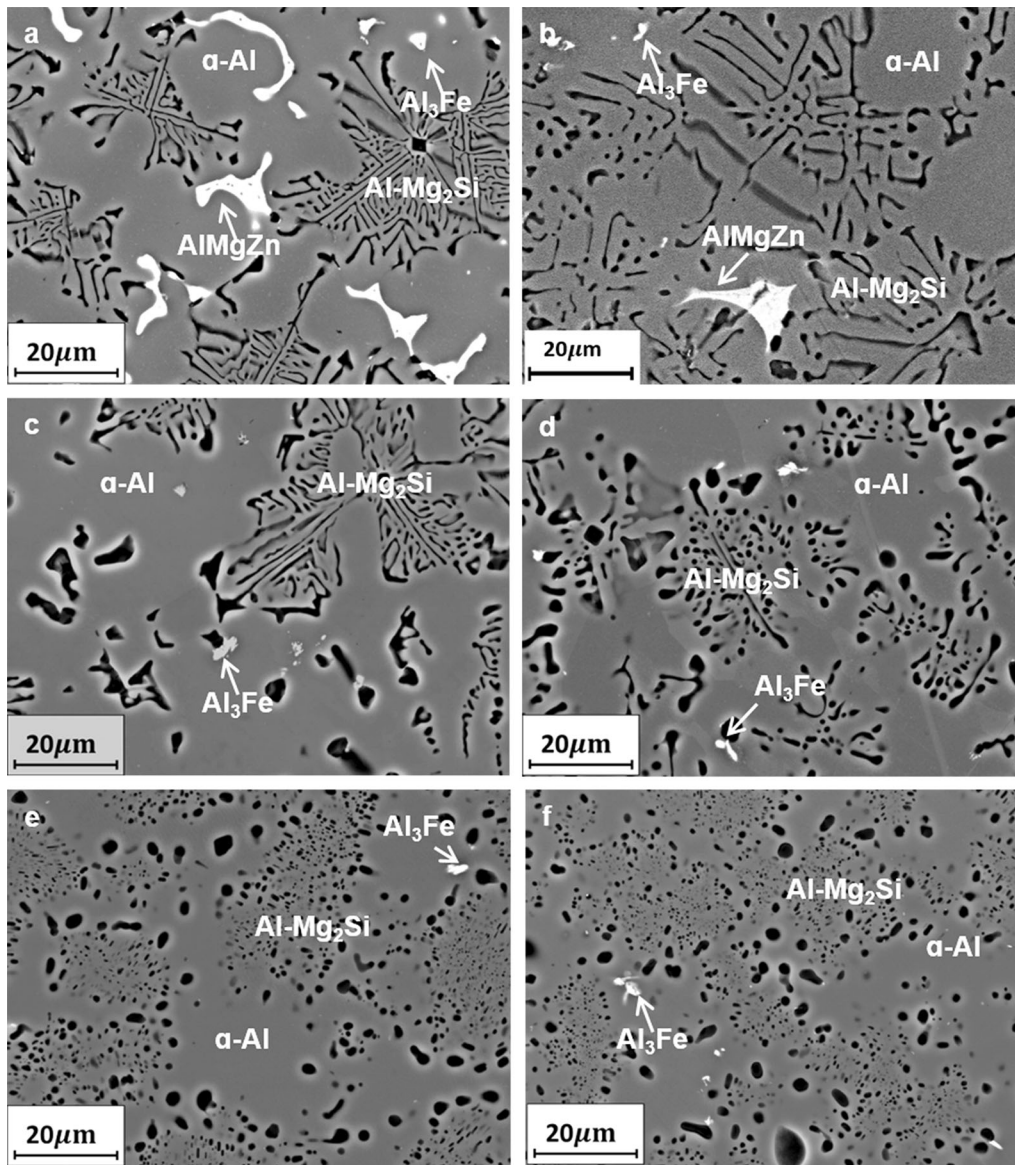


Fig. 9—Effect of solution treatment at 510 °C for (a) 0, (b) 10, (c) 30, (d) 60, (e) 180, and (f) 240 min on the microstructure of the Al-Mg-Si-Zn alloy with 3.59 wt pct Zn.

Subsequent aging of the solution-treated samples was performed at 180 °C for 90 minutes. The samples were examined by TEM, and the results are shown in Figures 12 and 13. In Figure 12, there is a grain boundary between the Mg₂Si particle in the eutectic and the Al matrix. Numerous precipitates form within the Al matrix. The diffraction patterns from precipitates [indicated by white dashed ellipses in Figure 13(b)] are typical diffraction streaks of the η' -MgZn₂ phase.^[27]

Figure 14 shows the effect of the Zn concentrations on the tensile properties of the Al-Mg-Si-Zn alloy after solution treatment at 510 °C for 180 minutes and subsequent aging at 180 °C for 90 minutes. Similar to the properties in the as-cast condition, increasing the Zn

concentrations results in an increase in the yield strength but a decrease in elongation. The values of the yield strength and UTS are significantly higher after solution treatment and aging. For the Al-Mg-Si-Zn alloy containing 3.59 wt pct Zn, after solution treatment at 510 °C for 180 minutes followed by aging at 180 °C for 90 minutes, the yield strength is 280 MPa, the UTS is 310 MPa, and the elongation is 1.74 pct. Compared to the values under the as-cast condition, the yield strength is 59 pct higher, the UTS is 37 pct higher, and the elongation is 81 pct higher. The results in Figure 14 also show that the properties can be tailored by varying the zinc concentration in the alloy, which is important for industrial applications, especially when high ductility is required.

IV. DISCUSSION

A. Solidification of the Al-Mg-Si-Zn Alloys

According to the equilibrium phase diagram calculated using Pandat software (Figure 15), intermetallic phases form as the Zn concentration of the Al-Mg-Si-Zn alloy increases. Figure 15 shows that the α -Al, Mg_2Si , β - Al_2Mg_3 and AlMgZn phases form after solidification with different Zn concentrations. The different phases and volume fractions calculated by the Scheil equation under nonequilibrium conditions are given in Table III. The volume fraction of the β - Al_2Mg_3 phase decreases, but that of the AlMgZn phase increases as the Zn concentration of the Al-Mg-Si-Zn alloy increases.

The calculated phase diagram in Figure 15 shows that the β - Al_2Mg_3 phase forms when the Zn content is less than 2.4 wt pct. With the increasing Zn concentration, formation of the β - Al_2Mg_3 phase is suppressed by precipitation of the stable τ - $Mg_{32}(Al, Zn)_{49}$ phase in the Al-Mg-Zn alloy.^[28] The volume fraction of the AlMgZn intermetallic initially increases and then stabilizes at

3.7 pct when the Zn content increases to 3.59 wt pct, although the average area of the AlMgZn intermetallic increases at high Zn concentration (4.62 wt pct). This can be explained by phase evolution of the AlMgZn intermetallic at different Zn concentrations. At low Zn content (< 1.01 wt pct), the ternary τ - $Mg_{32}(Al, Zn)_{49}$ phase precipitates during solidification. This stable τ phase distributes along the grain boundaries and inside the grains.^[29] With the increasing Zn content from 2.37 to 3.59 wt pct, the η' - $MgZn_2$ and ternary τ - $Mg_{32}(Al, Zn)_{49}$ phases form in the microstructure.^[30] At high Zn content (4.62 wt pct), only the η' - $MgZn_2$ phase is present based on the XRD results (Figure 7). The mechanical properties of the alloy are determined by its microstructure. Because of the irregular morphology and discontinuous distribution along the grain boundaries, the AlMgZn phase [η' - $MgZn_2$ and τ - $Mg_{32}(Al, Zn)_{49}$] inhibits crack initiation and accelerates crack propagation, which results in a decrease in the ductility but enhances the strength of the Al-Mg-Si-Zn alloy in the as-cast condition.^[31,32]

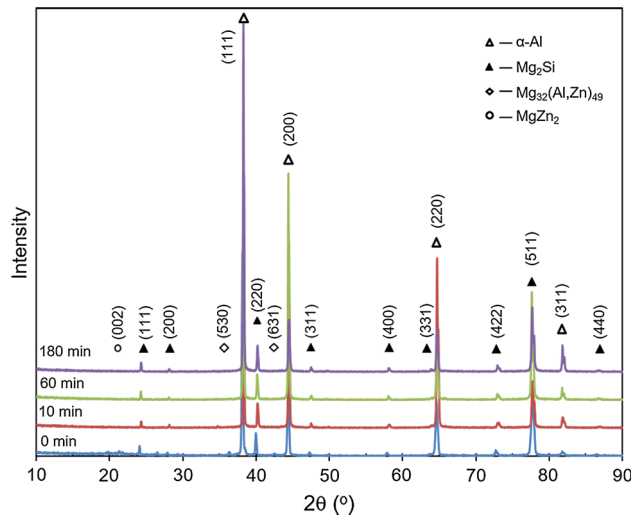


Fig. 10—XRD patterns of the Al-Mg-Si-Zn alloy with 3.59 wt pct Zn after solution treatment at 510 °C for different times.

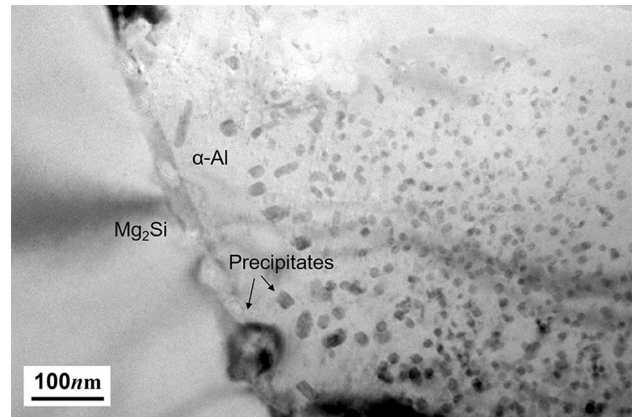


Fig. 12—Brightfield TEM image showing the different phases in the Al-Mg-Si-Zn alloy with 3.59 wt pct Zn after solution treatment at 510 °C for 180 min and aging at 180 °C for 90 min.

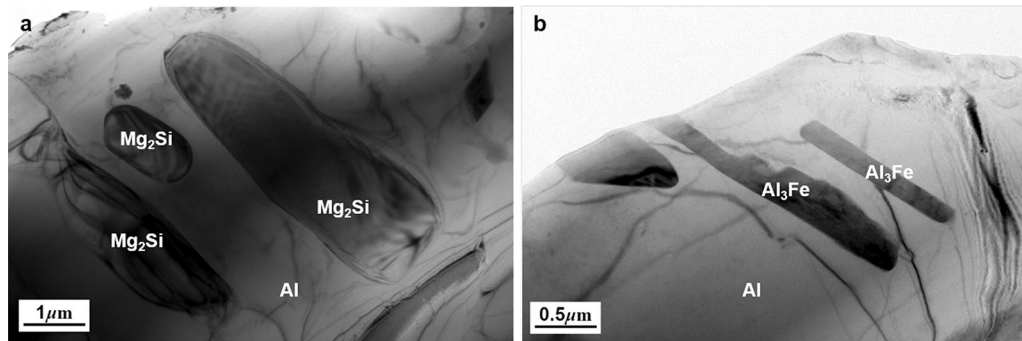


Fig. 11—TEM images showing the morphologies of (a) Mg_2Si particles and (b) the Fe-rich intermetallic phase in the Al-Mg-Si-Zn alloy with 3.59 wt pct Zn after solution treatment at 510 °C for 180 min.

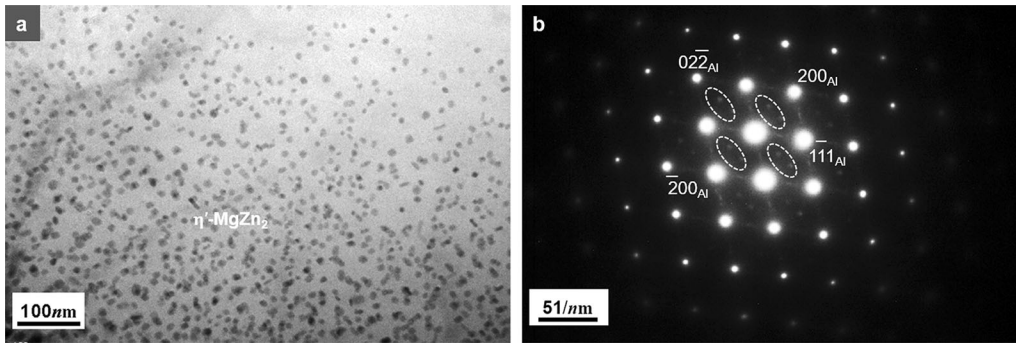


Fig. 13—(a) Brightfield TEM image in the $[011]_{Al}$ zone axis and (b) the corresponding selected area diffraction pattern of the η' - $MgZn_2$ precipitates in the Al-Mg-Si-Zn alloy with 3.59 wt pct Zn after solution treatment at 510 °C for 180 min and aging at 180 °C for 90 min.

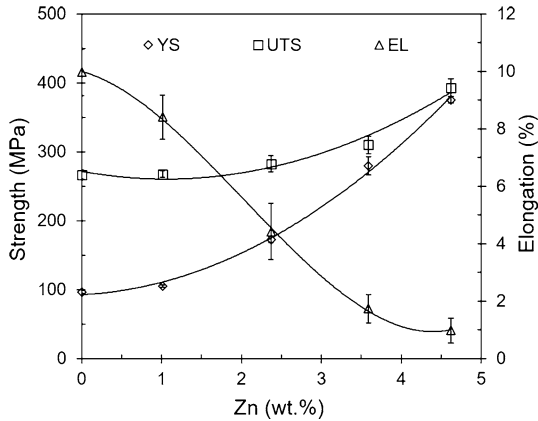


Fig. 14—Effect of the Zn content on the tensile properties of the Al-Mg-Si-Zn alloy after solution treatment at 510 °C for 180 min and subsequent aging at 180 °C for 90 min (YS = yield strength, UTS = ultimate tensile strength, EL = elongation).

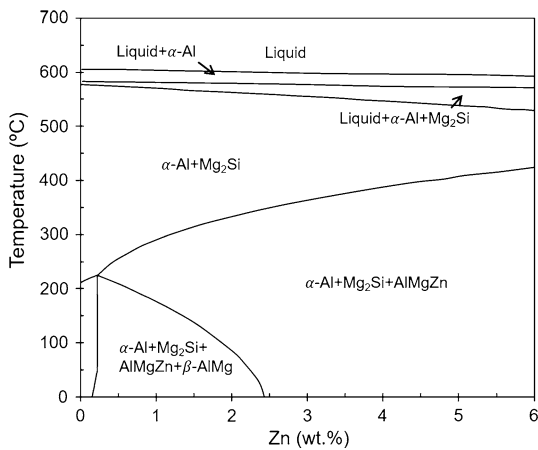


Fig. 15—Equilibrium phase diagram of the Al-Mg-Si-Zn alloy on the cross section of Al-8.0 wt pct Mg-Zn-2.6 wt pct Si calculated by Pandat software.

B. Heat Treatment of the Al-Mg-Si-Zn Alloys

With solution treatment at 510 °C for 30 minutes, the η' - $MgZn_2$ and τ - $Mg_{32}(Al, Zn)_{49}$ phases dissolve in the primary α -Al matrix. The behavior of the Mg_2Si phase is

Table III. Volume Fractions of the Different Phases in the Al-Mg-Si-Zn Alloys Calculated Using the Scheil Equation

Zn (Wt Pct)	0	1	2	3	4	5
α -Al Phase	37.7	37.1	36.8	36.3	35.7	35.2
Al + Mg_2Si Eutectic	60.5	60.8	60.9	61.0	61.2	61.4
β -AlMg Phase	1.8	1.2	0.4	0.2	0.1	0
AlMgZn Phase	0	0.9	1.9	2.5	3.0	3.4

different from that of the β - Mg_2Si precipitates in Al-Si-Mg alloys.^[33] This is because the Mg_2Si phase in quaternary Al-Mg-Si-Zn alloys has a limited concentration in the primary α -Al matrix, which is determined by the excess Mg content in pseudo-binary Al-Mg₂Si alloys.^[16]

A number of precipitates have been reported in Al-Mg-Zn-based alloys after heat treatment. Table IV summarizes the precipitates observed in Al-Mg-Zn-based alloys.^[12-14,27,31,32,34,35] η -Type precipitates are observed in alloys with magnesium concentration below 2.5 wt pct, while τ - $Mg_{32}(Al, Zn)_{49}$ phases are observed for relatively high magnesium concentration. A numerical model has also been established to prove that the τ phase exists with the increasing Mg content in Al-6 wt pct Zn-2 wt pct Cu-(1 to 4) wt pct Mg alloys.^[36] With the addition of silicon, the precipitates observed in Al-Zn-Mg-Si-based alloys are slightly different. The precipitates reported in the literature are given in Table V.^[20,21,30]

The precipitates observed in this study agree with those reported in the literature. This study reveals that the η' - $MgZn_2$ phase exists in the Al-8.1 wt pct Mg-2.6 wt pct Si-3.59 wt pct Zn alloy after heat treatment (solution treatment at 510 °C for 180 minutes, water quenching and then aging at 180 °C for 90 minutes). For AlZnMg alloys, the typical precipitate sequence is $\alpha \rightarrow GP \rightarrow \eta'$ - $MgZn_2 \rightarrow \eta$ - $MgZn_2$.^[12,14,27,35] Based on the brightfield TEM images shown in Figure 13, high-density short rod-shaped fine precipitates ranging in the size from 5 to 10 nm are observed in the microstructure, which has been confirmed to be the η' - $MgZn_2$ phase.^[27]

Table IV. Summary of the Precipitates Observed in Al-Zn-Mg-Based Alloys After Heat Treatment

Alloys	Mg (Wt Pct)	Zn (Wt Pct)	Precipitates	Refs.
Al-5.36Zn-1.21Mg	1.21	5.36	GP1, GP2	Berg <i>et al.</i> ^[34]
Al-5.48Zn-2.02Mg	2.02	5.48	η'	Li <i>et al.</i> ^[14]
Al-9.78Zn-2.04Mg-1.76Cu	2.04	9.78	η'	Wen <i>et al.</i> ^[12]
Al-4.21Zn-2.26Mg	2.26	4.21	η'	Zhao <i>et al.</i> ^[35]
Al-6.0Zn-2.3Mg-1.8Cu	2.30	6.00	η'	Yang <i>et al.</i> ^[27]
Al-7.6Zn-2.55Mg	2.55	7.60	τ	Yang <i>et al.</i> ^[13]
Al-(5.49 to 11.53)Mg-5.3Zn	5.49 to 11.53	5.30	τ	Pech-Canul <i>et al.</i> , Valdez <i>et al.</i> ^[31,32]

Table V. Summary of the Precipitates Observed in Al-Zn-Mg-Si-Based Alloys After Heat Treatment

Alloys	Mg (Wt Pct)	Zn (Wt Pct)	Si (Wt Pct)	Precipitates	Refs.
Al-0.66Mg-0.85Si-0.6Zn-0.2Cu	0.66	0.60	0.85	η' , β -Mg ₂ Si	Yan <i>et al.</i> ^[20]
Al-0.9Mg-0.5Si-3Zn	2.02	3.00	0.50	GP2, η' , β -Mg ₂ Si	Ding <i>et al.</i> ^[21]
Al-10.2Mg-3.2Zn-2.7Si	10.2	3.20	2.70	η'	Yang <i>et al.</i> ^[30]

Table VI. Mechanical Properties of Al-Mg-Zn-(Si) Alloys After Heat Treatment

Alloys	Mg (Wt Pct)	Zn (Wt Pct)	Si (Wt Pct)	Process	YS (MPa)	UTS (MPa)	EL (Pct)	Refs.
Al-9.78Zn-2.04Mg-1.76Cu	2.04	9.78	—	extrusion	654	702	12	Wen <i>et al.</i> ^[12]
Al-5.48Zn-2.02Mg	2.02	5.48	—	rolled sheet	561	581	10.1	Li <i>et al.</i> ^[14]
Al-11.0Mg-2.9Si-3.5Zn-0.6Mn	11.00	3.50	2.90	high-pressure die cast	300	420	3	Ji <i>et al.</i> ^[16]
Al-0.66Mg-0.85Si-0.2Cu-0.6Zn	0.66	0.60	0.85	rolled sheet	270	335	26.5	Yan <i>et al.</i> ^[20]

C. Mechanical Properties of the Al-Mg-Si-Zn Alloys

Several researchers have determined the mechanical properties of Al-Mg-Zn-based alloys after heat treatment, and the properties of the alloys are summarized in Table VI.^[12,14,16,20] The strength of the T6 temper is significantly affected by the zinc concentration. Both the yield strength and UTS decrease with the decreasing zinc content. Precipitate strengthening in Al-Mg-Zn-based alloys is strong and effective because of the small size and uniform distribution,^[37] which significantly enhances the strength of Al-Mg-Zn alloys.

In the current study, the Al-8.1 wt pct Mg-2.6 wt pct Si-3.59 wt pct Zn alloy processed by gravity die casting has a yield strength of 280 MPa, an UTS of 310 MPa and elongation of 1.74 pct. The property enhancement is closely associated with precipitate strengthening and spheroidization of the eutectic phases. As mentioned above, precipitate strengthening is effective. Spheroidization of the eutectic phase can inhibit creation of cracks under loading. Therefore, heat treatment is an important processing step for this material.

V. CONCLUSIONS

- (1) The as-cast microstructure of the Al-8.1 wt pct Mg-2.6 wt pct Si alloy consists of the primary α -Al phase, Al-Mg₂Si eutectic phase, and Al₃Fe phase. The AlMgZn intermetallic phase forms when Zn is added to the ternary alloy. When the Zn content is 1.01 wt pct, the τ -Mg₃₂(Al, Zn)₄₉ phase forms in the microstructure, whereas the τ -Mg₃₂(Al, Zn)₄₉ and η -MgZn₂ phases precipitate when the Zn content is 2.37 or 3.59 wt pct. The η -MgZn₂ phase is present when the Zn content is 4.62 wt pct.
- (2) The τ -Mg₃₂(Al, Zn)₄₉ and η -MgZn₂ phases strengthen the Al-Mg-Si alloy over a range of Zn contents. With a Zn content of 3.59 wt pct, the mechanical properties under the as-cast condition are a yield strength of 176 MPa, an UTS of 225 MPa, and elongation of 1.06 pct.
- (3) When solution treatment is performed at 510 °C for 30 minutes, the τ -Mg₃₂(Al, Zn)₄₉ and η -MgZn₂ phases in the Al-8.1 wt pct Mg-2.6 wt pct Si-3.59 wt pct Zn alloy rapidly

dissolve in the α -Al matrix, but no obvious spheroidization of the Mg_2Si phase occurs for this short treatment time. When the solution treatment time is increased to 180 minutes, the lamellar Mg_2Si phase spheroidizes to compact and nodular shapes.

- (4) After aging at 180 °C for 90 minutes, high-density fine precipitates of the η' - MgZn_2 phase form in the α -Al matrix. The η' - MgZn_2 precipitates improve the strength of the Al-Mg-Si-Zn alloy after heat treatment. The mechanical properties of the alloy containing 3.59 wt pct Zn are a yield strength of 280 MPa, an UTS of 310 MPa and elongation of 1.74 pct.

ACKNOWLEDGMENTS

Financial supports from the EPSRC Impact Acceleration Accounts (IAA) United Kingdom (Project Number R33044), Shenzhen Free Exploring Basic Research Project (JCYJ20170307110223452), the National Natural Science Foundation of China (51501152), and the Natural Science Basic Research Plan of Shaanxi Province, China (2016JQ5093) are gratefully appreciated. Mr. L. Li also thanks Liwen Bianji, Edanz Group China (www.liwenbianji.cn/ac), for editing the English text of a draft of this manuscript.

OPEN ACCESS

This article is distributed under the terms of the Creative Commons Attribution 4.0 International License (<http://creativecommons.org/licenses/by/4.0/>), which permits unrestricted use, distribution, and reproduction in any medium, provided you give appropriate credit to the original author(s) and the source, provide a link to the Creative Commons license, and indicate if changes were made.

REFERENCES

1. K. Alan: *Die Casting Metallurgy*, 1st ed., Butterworths and Co., London, 1982, pp. 10–14.
2. D.M. Stefanescu: *Casting. ASM Handbook*, ASM International, Novato, OH, 2008, vol. 15, pp. 585–611.
3. J. Hirsch: *Mater. Trans.*, 2011, vol. 52, pp. 818–24.
4. L. Ceschini, A. Morri, A. Morri, and G. Pivetti: *Mater. Des.*, 2011, vol. 32, pp. 1367–75.
5. I. Polmear: *Light Alloys*, 4th ed., Butterworth-Heinemann, Oxford, 2005, pp. 220–26.

6. J.G. Kaufman and E.L. Rooy: *Aluminum Alloy, Castings, Properties, Processes, and Applications*, ASM International, Novato, OH, 2004, pp. 13–57.
7. P. Ouellet and F.H. Samuel: *J. Mater. Sci.*, 1999, vol. 34, pp. 4671–97.
8. A. Wiengmoon, J.T.H. Pearce, T. Chairuangsrir, S. Isodad, H. Saitoe, and H. Kurata: *Micron*, 2013, vol. 45, pp. 32–36.
9. R. Jahn, W.T. Donlon, and J.E. Allison: *Proc. Symp. TMS Annu. Meet. Automot. Alloys 1999*, 1999, pp. 247–64.
10. J.Y. Hwang, R. Banerjee, H.W. Doty, and M.J. Kaufman: *Acta Mater.*, 2009, vol. 57, pp. 1308–17.
11. R.K. Mishra, G.W. Smith, W.J. Baxter, A.K. Sachdev, and V. Franetovic: *J. Mater. Sci.*, 2001, vol. 36, pp. 461–68.
12. K. Wen, Y. Fan, G. Wang, L. Jin, X. Li, Z. Li, Y. Zhang, and B. Xiong: *Mater. Des.*, 2016, vol. 101, pp. 16–23.
13. X. Yang, J.H. Chen, J.Z. Liu, F. Qin, J. Xie, and C.L. Wu: *J. Alloys Compd.*, 2014, vol. 610, pp. 69–73.
14. B. Li, Q. Pan, C. Chen, H. Wu, and Z. Yin: *J. Alloys Compd.*, 2016, vol. 664, pp. 553–64.
15. S.-S. Shin, K.-M. Lim, and I.-M. Park: *J. Alloys Compd.*, 2016, vol. 671, pp. 517–26.
16. S. Ji, F. Yan, and Z. Fan: *Mater. Sci. Eng. A*, 2015, vol. 626, pp. 165–74.
17. S. Ji, F. Yan, Z. Fan: *Light Metals*, 2016, pp. 207–10. <https://doi.org/10.1007/978-3-319-48251-4>.
18. F. Yan, W. Yang, S. Ji, and Z. Fan: *Mater. Chem. Phys.*, 2015, vol. 167, pp. 88–96.
19. S. Ji, F. Yan, and Z. Fan: *Mater. Sci. Forum*, 2015, vols. 828–829, pp. 9–14.
20. L. Yan, Y. Zhang, X. Li, Z. Li, F. Wang, H. Liu, and B. Xiong: *Prog. Nat. Sci. Mater. Int.*, 2014, vol. 24, pp. 97–100.
21. X. Ding, H. Cui, J.X. Zhang, H.X. Li, M.X. Guo, Z. Lin, L.Z. Zhuang, and J.S. Zhang: *Mater. Des.*, 2015, vol. 65, pp. 1229–35.
22. C.A. Aliravci and M.Ö. Pekgülyüz: *CALPHAD Comput. Coupling Phase Diagr. Thermochem.*, 1988, vol. 22, pp. 147–55.
23. S. Kumar and K.A.Q. O'Reilly: *Mater. Charact.*, 2016, vol. 120, pp. 311–22.
24. S. Belmares-Perales and A.A. Zaldivar-Cadena: *Mater. Sci. Eng. B*, 2010, vol. 174, pp. 191–95.
25. J. Song, Z. Wang, Y. Huang, A. Srinivasan, F. Beckmann, K.U. Kainer, and N. Hort: *Mater. Des.*, 2015, vol. 87, pp. 157–70.
26. Y. Wang, Q. Wang, G. Wu, Y. Zhu, and W. Ding: *Mater. Lett.*, 2002, vol. 57, pp. 929–34.
27. W. Yang, S. Ji, M. Wang, and Z. Li: *J. Alloys Compd.*, 2014, vol. 610, pp. 623–29.
28. M.C. Carroll, P.I. Gouma, M.J. Mills, G.S. Daehn, and B.R. Dunba: *Scripta Mater.*, 2000, vol. 42, pp. 335–40.
29. C. Meng, D. Zhang, H. Cui, L. Zhuang, and J. Zhang: *J. Alloys Compd.*, 2014, vol. 617, pp. 925–32.
30. W. Yang, L. Liu, J. Zhang, and S. Ji: *Mater. Sci. Eng. A*, 2017, vol. 682, pp. 85–89.
31. M.I. Pech-Canul, A. Bautista-Hernandez, M. Salazar-Villanueva, and S. Valdez: *Mater. Des.*, 2013, vol. 44, pp. 325–30.
32. S. Valdez, J. Genesca, B. Campillo, O. Flores, R. Perez, and J.A. Juarez-Islas: *Mater. Lett.*, 2008, vol. 62, pp. 1139–42.
33. X. Dong, Y. Zhang, and S. Ji: *Mater. Sci. Eng. A*, 2017, vol. 700, pp. 291–300.
34. L.K. Berg, J. Gjønnnes, V. Hansen, X.Z. Li, M. Knutson-Wedel, G. Waterloo, D. Schryvers, and L.R. Wallenberg: *Acta Mater.*, 2001, vol. 49, pp. 3443–51.
35. X. Zhao, C. Chen, and F. Chen: *Mater. Lett.*, 2017, vol. 188, pp. 95–98.
36. P. Priya, D.R. Johnson, and M.J.M. Krane: *Comput. Mater. Sci.*, 2017, vol. 139, pp. 273–84.
37. S. Zhang, W. Hu, R. Berghammer, and G. Gottstein: *Acta Mater.*, 2010, vol. 58, pp. 6695–6705.